

Topological magnons in a Kagome lattice spin system with XXZ and Dzyaloshinskii-Moriya interactions

Ranjani Seshadri and Diptiman Sen

Centre for High Energy Physics, Indian Institute of Science, Bengaluru 560 012, India

(Dated: October 13, 2018)

We study the phases of a spin system on the Kagome lattice with nearest-neighbor XXZ interactions with anisotropy ratio Δ and Dzyaloshinskii-Moriya interactions with strength D . In the classical limit where the spin S at each site is very large, we find a rich phase diagram of the ground state as a function of Δ and D . There are five distinct phases which correspond to different ground state spin configurations in the classical limit. We use spin wave theory to find the bulk energy bands of the magnons in some of these phases. We also study a strip of the system which has infinite length and finite width; we find modes which are localized on one of the edges of the strip with energies which lie in the gaps of the bulk modes. In the ferromagnetic phase in which all the spins point along the $+\hat{z}$ or $-\hat{z}$ direction, the bulk bands are separated from each other by finite energy gaps. This makes it possible to calculate the Berry curvature at all momenta, and hence the Chern numbers for every band; the number of edge states is related to the Chern numbers. Interestingly, we find that there are four different regions in this phase where the Chern numbers are different. Hence there are four distinct topological phases even though the ground state spin configuration is identical in all these phases. We calculate the thermal Hall conductivity of the magnons as a function of the temperature in the above ferromagnetic phase; we find that this can distinguish between the various topological phases. These results are valid for all values of S . In the other phases, there are no gaps between the different bands; hence the edge states are not topologically protected.

I. INTRODUCTION

For the last several years topological phases of matter have been studied extensively in a variety of systems both theoretically and experimentally^{1–3}. A hallmark of such systems is that the energy bands of the bulk modes have gaps, and there are modes which lie at the edges of the system and whose energies lie in the gaps of the bulk bands. In addition, these systems have a bulk-boundary correspondence; the bulk bands are characterized by some topological invariants which are integers, and these give the number of edge modes with a given momentum.

A relatively new entrant to the class of topological systems are spin systems where the objects of interest are magnons (spin waves)^{4–16}. It has been shown in a variety of such systems that there are topological phases in which the bulk bands of the magnons are gapped with respect to each other, and they have non-zero values of some topological invariants which give the number of edge modes at the boundaries of finite-sized systems. The different topological phases typically have different ground states.

In this paper, we will present our studies of a spin system in which there are several topological phases of magnons all of which have the same ground state. The system consists of spins on a Kagome lattice with anisotropic XXZ and Dzyaloshinskii-Moriya interactions^{17,18} between nearest-neighbor spins. We will show that the different topological phases can be distinguished from each other through the temperature dependence of

the thermal Hall conductivity^{19,20}. These results turn out to be valid for any value of the spin.

The plan of the paper is as follows. In Sec. II, we introduce a model of spins on a Kagome lattice with nearest-neighbor XXZ interactions with anisotropy ratio Δ and a Dzyaloshinskii-Moriya interactions with strength D . In the classical limit in which the spin $S \rightarrow \infty$, we find the ground states over a wide range of Δ and D . We discover that there are five different phases numbered I to V which are separated pairwise by phase transition lines. Of these, phase I is the simplest; here the ground state consists of all spins pointing in the $+\hat{z}$ or $-\hat{z}$ direction. In the ground state of phase II , all the spins point in the same direction which can be along any direction in the $x - y$ plane. In phases III and IV , the three spins in each triangle of the Kagome lattice form a configuration in which they lie in the $x - y$ plane at angles which differ from each other by $2\pi/3$ in a clockwise or anticlockwise sense. The ground state in phase V has the most complex spin configuration. In Sec. III, we study linear spin wave theory in phase I by using the Holstein-Primakoff transformation and expanding the Hamiltonian to the next order in a $1/S$ expansion. Since the unit cell of the Kagome lattice consists of three spins forming a triangle, spin wave theory gives three bands of magnon energies. We find that the bands are all separated from each other by gaps. This allows us to calculate the Berry curvature in each band for all values of the momentum in the Brillouin zone. Integrating the Berry curvature gives the Chern numbers of the different bands. We then find that

phase *I* consists of four distinct topological phases; these are separated from each other by lines where the gaps between pairs of bands vanish. Next we consider a strip of the Kagome lattice which is infinitely long and has a finite width. We discover that there are magnons which are localized along one of the two edges of the strip; the energies of these edge magnons lie in the gaps of the bulk bands. The number of edge magnons is closely related to the Chern numbers. We then calculate the thermal Hall conductivity and show that it has different values in the different topological phases. All these results turn out to be valid for all values of S . In Sec. IV, we study spin wave theory in phases *II* and *III*. The three magnon bands are not separated from each other by gaps in these phases. Hence the Berry curvatures are ill-defined at certain momenta and the Chern numbers cannot be calculated. Although edge states appear in these phases also, they are not topologically protected. In Sec. V we summarize our results and point out some directions for future studies.

II. SPINS ON A KAGOME LATTICE WITH XXZ AND DZHALOSHINSKII-MORIYA INTERACTIONS

We consider a system of spins on a Kagome lattice with XXZ and Dzyaloshinskii-Moriya interactions (DMI) between nearest neighbors. A schematic picture of the system is shown in Fig. 1(a). The unit cell of the Kagome lattice is given by a triangle consisting of sites A , B and C as shown. We will denote the coordinates of a unit cell by $\vec{n} = (n_1, n_2)$, and the spin operators at the three sites by $A_{\vec{n}}$, $B_{\vec{n}}$ and $C_{\vec{n}}$ respectively. The Hamiltonian of the system is a sum of the XXZ interactions (H_{Δ}) and DMI (H_{DM}), where

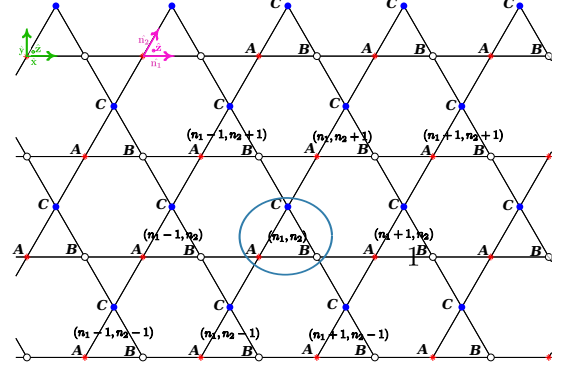
$$H = H_{\Delta} + H_{DM}, \quad (1)$$

$$H_{\Delta} = - \sum_{\langle \vec{n}\vec{n}' \rangle} J_{\alpha} (A_{\vec{n}}^{\alpha} B_{\vec{n}'}^{\alpha} + B_{\vec{n}}^{\alpha} C_{\vec{n}'}^{\alpha} + C_{\vec{n}}^{\alpha} A_{\vec{n}'}^{\alpha}),$$

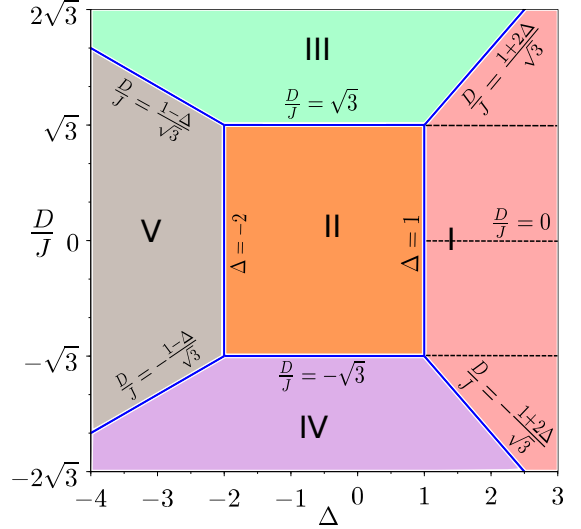
$$H_{DM} = D \hat{\mathbf{z}} \cdot \sum_{\langle \vec{n}\vec{n}' \rangle} (\vec{A}_{\vec{n}} \times \vec{B}_{\vec{n}'} + \vec{B}_{\vec{n}} \times \vec{C}_{\vec{n}'} + \vec{C}_{\vec{n}} \times \vec{A}_{\vec{n}'}),$$

$$\text{where } J_{\alpha} = \begin{cases} J & \text{if } \alpha = x \text{ or } y, \\ \Delta J & \text{if } \alpha = z, \end{cases}$$

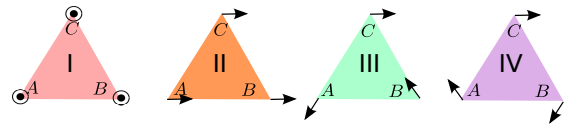
and $\langle \vec{n}\vec{n}' \rangle$ denotes nearest-neighbor pairs. The Hamiltonian has two parameters, the anisotropy ratio Δ which is dimensionless and the DMI strength D (the ratio D/J is dimensionless, hence we will often use this parameter below). For $\Delta = 1$, H_{Δ} describes an isotropic ferromagnet. We note that both the terms in the Hamiltonian in Eq. (1) are invariant under arbitrary spin rotations in



(a) Kagome lattice



(b) Phase diagram



(c) Spin configurations

FIG. 1: A Kagome lattice can be viewed as a triangular lattice of unit cells each of which is also a triangle with three sites labeled A , B and C . One of the unit cells is shown as a blue circle in (a). The geometry shown in (a) is used for our edge state calculations; thus the bottom edge is a straight edge whereas the top edge is jagged. The top left corner (in green) shows the coordinate axes. Adjacent to it (in magenta) is shown the non-orthogonal $n_1 - n_2$ coordinate axes used for our calculations. The z -axis points out of the plane. Classically the system has five phases shown in different colors in (b); the corresponding spin orientations in the ground state are shown in (c). Although phase *I* (red) is a single phase in terms of the ground state spin configuration, it consists of four distinct topological phases which are separated from each other by the dotted horizontal lines $D/J = 0, \pm\sqrt{3}$.

the $x-y$ plane, i.e., around the \hat{z} axis. We will see below that this continuous symmetry has implications for the magnon energy spectrum in some of the phases.

The system described in Eq. (1) becomes classical in the limit that the spin $S \rightarrow \infty$, where $\vec{A}_{\vec{n}}^2 = \vec{B}_{\vec{n}}^2 = \vec{C}_{\vec{n}}^2 = S(S+1)\hbar^2$. In this limit we can find the ground state spin configuration as follows. We assume that in the ground state, all the unit cells (i.e., triangles) look identical. This means that the ground state of the full Kagome lattice is the same as that of the three spins at the vertices of a triangle. Classically, we can write the components of $\vec{A}_{\vec{n}}, \vec{B}_{\vec{n}}$ and $\vec{C}_{\vec{n}}$ in terms of the polar coordinates θ and ϕ . Since the Hamiltonian is invariant under spin rotations in the $x-y$ plane, we can choose, say, $\phi_C = 0$. We will therefore write

$$\begin{aligned}\vec{A}_{\vec{n}} &= S(\sin \theta_A \cos \phi_A, \sin \theta_A \sin \phi_A, \cos \theta_A), \\ \vec{B}_{\vec{n}} &= S(\sin \theta_B \cos \phi_B, \sin \theta_B \sin \phi_B, \cos \theta_B), \\ \vec{C}_{\vec{n}} &= S(\sin \theta_C, 0, \cos \theta_C),\end{aligned}\quad (2)$$

for all values of \vec{n} . We thus have to consider five parameters, $p_i = \theta_A, \theta_B, \theta_C, \phi_A, \phi_B$. We then numerically find the spin configuration which minimizes the energy of the Hamiltonian given in Eq. (1) for different values of the five parameters. We find five phases as shown in Fig. 1(b). In phase *I*, all the spins point along the $+\hat{z}$ (or $-\hat{z}$) direction; this is a ferromagnetic configuration along the \hat{z} axis. In phase *II*, all the spins point along the \hat{x} direction (this direction is fixed due to our choice $\phi_C = 0$); hence we have a ferromagnetic configuration along the \hat{x} direction. Thus both phases *I* and *II* have collinear spin configurations. In phase *III*, the spins again lie in the $x-y$ plane, but they rotate by $2\pi/3$ in the clockwise direction as we go around the triangle from *A* to *B* to *C* (see Fig. 1(c)). In phase *IV*, the spins lie in the $x-y$ plane and rotate by $2\pi/3$ in the anticlockwise direction as we go around the triangle. Thus phases *III* and *IV* have coplanar configurations. (We can see from Eq. (1) that $D \rightarrow -D$ is equivalent to carrying out the unitary transformation $S_i^y \rightarrow -S_i^y$, $S_i^z \rightarrow -S_i^z$, and $S_i^x \rightarrow S_i^x$ on every site i , namely, rotating by π around the \hat{x} axis. We can see that from Fig. 1(c) that this transformation changes the spin configuration in phase *III* to that in phase *IV*). In phase *V*, the spins do not necessarily lie in the same plane; this makes it difficult to study this phase analytically.

In Fig. 1(b), the phase transition (PT) lines lying between two of the four phases *I*, *II*, *III* and *IV* are lines on which the ground state energies of the two appropriate phases are equal. We can find out as follows if these lines correspond to a PT of first order or higher order. We calculate the first derivative of the ground state energy along a line which crosses a PT line perpendicularly. If the derivative approaches different values as we approach

the transition line from the two sides, it corresponds to a first order transition; otherwise we call it a higher order transition. We find that all the PT lines between phases *I* – *IV* are of first order. However, this method cannot be used to characterize the PT lines lying between phase *V* and the phases *II* – *IV*. Since we do not have an analytical expression for the ground state energy in phase *V*, we do not know what its first derivative is when we approach one of its PT lines.

Next, we can study the stability of phases *I* – *IV*. To do this, we slightly perturb the five parameters p_i away from their ground state values. We then find the matrix of second derivatives of the ground state energy; the entries of this matrix are given by $S_{ij} = \partial^2 E_0 / \partial p_i \partial p_j$. If all the eigenvalues of this matrix are positive, the phase is stable; if any one of the eigenvalues is negative, it is unstable. We find that the phases *I* – *IV* are stable in the regions shown for them in Fig. 1(b). This method gives the PT transition lines between the phases *II* – *IV* and phase *V*; those are the lines where one of the eigenvalues of S_{ij} calculated in phases *II*, *III*, *IV* becomes zero.

To give a simple example of the calculations mentioned above, we look at the neighborhood of the line $\Delta = 1$ in Fig. 1(b) which lies between phases *I* and *II*. We consider a ferromagnetic spin configuration given by $\phi_A = \phi_B = \phi_C = 0$ and $\theta_A = \theta_B = \theta_C = \theta$. For this configuration, the energy of a single triangle is given by

$$E(\theta) = -3JS^2(\Delta \cos^2 \theta + \sin^2 \theta). \quad (3)$$

For $\Delta > 1$, $E(\theta)$ has a minimum value of $E_0 = -3JS^2\Delta$ at $\theta = 0$ or π which corresponds to all the spins pointing along the $+\hat{z}$ or $-\hat{z}$ direction (phase *I*), while for $\Delta < 1$, $E(\theta)$ has a minimum value of $E_0 = -3JS^2$ at $\theta = \pi/2$ which corresponds to spins pointing along the $+\hat{x}$ direction (phase *II*). The two ground state energies match at $\Delta = 1$, but $\partial E_0 / \partial \Delta$, which is equal to $-3JS^2$ and zero in phases *I* and *II*, do not match at $\Delta = 1$. Hence the PT on the line $\Delta = 1$ is of first order. To examine the stability of phase *I*, we note from Eq. (3) that if θ is changed from zero to ϵ (where ϵ is small), the energy becomes $-3JS^2(\Delta - \Delta\epsilon^2 + \epsilon^2)$. Hence $\partial^2 E_0 / \partial \epsilon^2 = 6JS^2(\Delta - 1)$. This is positive and therefore phase *I* is stable if $\Delta > 1$. To examine phase *II*, we change θ from $\pi/2$ to $\pi/2 + \epsilon$. The energy is then given by $-3JS^2(1 - \epsilon^2 + \Delta\epsilon^2)$. Hence $\partial^2 E_0 / \partial \epsilon^2 = 6JS^2(1 - \Delta)$. Thus phase *II* is stable if $\Delta < 1$.

In the following sections we will use spin wave theory to study the properties of magnons in phases *I* – *IV*, both in the bulk and at the edges of an infinitely long strip of the system.

III. SPIN WAVE ANALYSIS IN PHASE I

The classical ground state in this phase has all the three spins pointing along the $+\hat{z}$ or $-\hat{z}$ direction; for definiteness, we will take them to point along $+\hat{z}$. To calculate the magnon spectrum in this phase, we use the Holstein-Primakoff transformation²¹. We write the spin operators in terms of bosonic creation and annihilation operators as

$$\begin{aligned} A_{\vec{n}}^z &= S - a_{\vec{n}}^\dagger a_{\vec{n}}, \\ A_{\vec{n}}^+ &= A_{\vec{n}}^x + iA_{\vec{n}}^y \simeq \sqrt{2S} a_{\vec{n}}, \\ A_{\vec{n}}^- &= A_{\vec{n}}^x - iA_{\vec{n}}^y \simeq \sqrt{2S} a_{\vec{n}}^\dagger, \end{aligned} \quad (4)$$

where $a_{\vec{n}}^\dagger$ and $a_{\vec{n}}$ are the bosonic creation and annihilation operators at the site denoted by $\vec{n} = (n_1, n_2)$. The last two equations hold in the limit of large S . We have similar transformations for the spin operators $B_{\vec{n}}$ and $C_{\vec{n}}$. Next, we Fourier transform to momentum space

$$(a, b, c)_{\vec{n}} = \sum_{\vec{k}} (a, b, c)_{\vec{k}} e^{i\vec{k} \cdot \vec{n}}, \quad (5)$$

where the sum over \vec{k} goes over the Brillouin zone (BZ) of the triangular lattice formed by the unit cells of the Kagome lattice. Retaining terms only up to second order in the bosonic operators, we obtain a spin wave Hamiltonian of the form

$$H = S \sum_{\vec{k}} \begin{pmatrix} a_{\vec{k}}^\dagger & b_{\vec{k}}^\dagger & c_{\vec{k}}^\dagger \end{pmatrix} h(\vec{k}) \begin{pmatrix} a_{\vec{k}} \\ b_{\vec{k}} \\ c_{\vec{k}} \end{pmatrix}, \quad (6)$$

where the 3×3 matrix $h(\vec{k})$ has the form

$$h(\vec{k}) = \begin{pmatrix} 4\Delta & -\mathcal{D}f(-k_1) & -\mathcal{D}^*f(-k_2) \\ -\mathcal{D}^*f(k_1) & 4\Delta & -\mathcal{D}f(k_1 - k_2) \\ -\mathcal{D}f(k_2) & -\mathcal{D}^*f(k_2 - k_1) & 4\Delta \end{pmatrix}, \quad (7)$$

with

$$\begin{aligned} \mathcal{D} &= 1 + \frac{iD}{J}, \\ f(k) &= 1 + e^{ik} = f^*(-k). \end{aligned} \quad (8)$$

(Since we have taken out a factor of S in Eq. (6), the magnon energies will be equal to S times the energies that we obtain from Eqs. (6-7). For convenience, we will not show this factor of S in the various figures below). Note that we have written $h(\vec{k})$ in terms of the momenta k_1 and k_2 which are along the directions of the unit vectors

\hat{n}_1 and \hat{n}_2 as shown in Fig. 1(a). These are related to the x and y momenta as $k_x = k_1/\sqrt{3}$ and $k_y = (2k_2 - k_1)/3$.

Since the Hamiltonian in Eqs. (6-7) is number conserving (i.e., there are only terms like $a^\dagger a$ and no terms like $a^\dagger a^\dagger$, so that the Hamiltonian commutes with $\sum_{\vec{k}} (a_{\vec{k}}^\dagger a_{\vec{k}} + b_{\vec{k}}^\dagger b_{\vec{k}} + c_{\vec{k}}^\dagger c_{\vec{k}})$), the magnon spectrum can be obtained by directly diagonalizing $h(\vec{k})$. (This is in contrast to the spin wave Hamiltonians in phases *II* and *III* which have terms like $a^\dagger a^\dagger$ and are therefore more difficult to diagonalize as we will see later). The eigenvalues of $h(\vec{k})$ are given by solutions to the cubic equation

$$\left(\frac{E}{S} - 4\Delta\right)^3 + a\left(\frac{E}{S} - 4\Delta\right) + b = 0, \quad (9)$$

where

$$\begin{aligned} a &= -2 \left(1 + \frac{D^2}{J^2}\right) \left(3 + \cos(k_1) + \cos(k_2) + \cos(k_1 - k_2)\right), \\ b &= 4 \left(1 + \cos(k_1) + \cos(k_2) + \cos(k_1 - k_2)\right). \end{aligned} \quad (10)$$

We can find the boundaries of phase *I* by examining where the magnon energy becomes zero. We find that at $\vec{k} = (0, 0)$, $h(\vec{k})$ in Eq. (7) has an eigenvalue equal to $4(\Delta - 1)$ with eigenvector $(1, 1, 1)^T$ (where the superscript T means transpose), and an eigenvalue $4\Delta + 2 - 2\sqrt{3}|D/J|$ corresponding to the eigenvector $(1, e^{-i2\pi/3}, e^{i2\pi/3})^T$ if $D > 0$ and $(1, e^{i2\pi/3}, e^{-i2\pi/3})^T$ if $D < 0$. We see that these eigenvalues touch zero when $\Delta = 1$ and $|D/J| = (1 + 2\Delta)/\sqrt{3}$. This gives the boundaries of phase *I* as shown in Fig. 1(b).

A. Discrete symmetries

There is a discrete set of transformations under which the Hamiltonian in Eq. (7) behaves in a simple way. Let us remove the diagonal part given by $4\Delta I$ and denote the rest of the Hamiltonian by $h'(\vec{k}, D/J)$. Namely,

$$h(\vec{k}, \frac{D}{J}) = h'(\vec{k}) - 4\Delta I. \quad (11)$$

We now define a 3×3 unitary and diagonal matrix U whose diagonal entries are given by $(1, e^{i2\pi/3}, e^{i4\pi/3})$; this generates a finite group with elements given by (I, U, U^2) . We then find that

$$\begin{aligned} U h'(\vec{k}, \frac{D}{J}) U^{-1} &= \left(-\frac{1}{2} + \frac{\sqrt{3}D}{2J}\right) h'(\vec{k}, \frac{\frac{D}{J} + \sqrt{3}}{1 - \frac{\sqrt{3}D}{J}}), \\ U^2 h'(\vec{k}, \frac{D}{J}) U^{-2} &= \left(-\frac{1}{2} - \frac{\sqrt{3}D}{2J}\right) h'(\vec{k}, \frac{\frac{D}{J} - \sqrt{3}}{1 + \frac{\sqrt{3}D}{J}}). \end{aligned} \quad (12)$$

[One can interpret these transformations as rotations by $\pm 2\pi/3$ in the two-dimensional plane defined by points with coordinates $(1, D/J)$]. Since the eigenvalues of a matrix are invariant under unitary transformations, Eq. (12) implies that the eigenvalues of $h'(\vec{k}, D/J)$, denoted as $E'_i(\vec{k}, D/J)$ (where $i = 1, 2, 3$ denotes the three bands), satisfy the relations

$$\begin{aligned} E'_i(\vec{k}, \frac{D}{J}) &= (-\frac{1}{2} + \frac{\sqrt{3}D}{2J}) E'_i(\vec{k}, \frac{\frac{D}{J} + \sqrt{3}}{1 - \frac{\sqrt{3}D}{J}}) \\ &= (-\frac{1}{2} - \frac{\sqrt{3}D}{2J}) E'_i(\vec{k}, \frac{\frac{D}{J} - \sqrt{3}}{1 + \frac{\sqrt{3}D}{J}}). \end{aligned} \quad (13)$$

Thus there are sets of three values of D/J such that the energies $E'_i(\vec{k}, D/J)$ are related to each other by some constants which do not depend on \vec{k} ; such sets of values of D/J will therefore share some properties of the energy bands (for instance, two of the bands touching each other at some value of \vec{k}). In particular, setting $D/J = 0$, we see that

$$\begin{aligned} E'_i(\vec{k}, 0) &= -\frac{1}{2} E'_i(\vec{k}, \sqrt{3}) \\ &= -\frac{1}{2} E'_i(\vec{k}, -\sqrt{3}). \end{aligned} \quad (14)$$

We will see below that there is no gap between the bottom and middle bands and also between the middle and top bands at both $D/J = 0$ and $\pm\sqrt{3}$; this is consistent with Eq. (14).

B. Energy spectrum of magnons

In phase *I*, the symmetry of the Hamiltonian under spin rotations in the $x - y$ plane is not broken by the ground state. We therefore do not expect a zero energy Goldstone mode. We indeed find that the magnon modes have strictly positive energy for all momenta \vec{k} .

In the absence of the DMI, i.e., for $D = 0$, we get a dispersionless top band. Secondly, we find that there are no gaps between any pair of bands. The bottom and middle bands (labeled 1 and 2 respectively) touch at two momenta in the Brillouin zone, $\vec{k} = \pm(2\pi/(3\sqrt{3}), -2\pi/3)$, while the middle and top (labeled 3) bands touch at $\vec{k} = (0, 0)$. The spectrum is also gapless at $D/J = \pm\sqrt{3}$. However, the gap closing points are now inverted, i.e., bands 1 and 2 touch at $\vec{k} = (0, 0)$, whereas bands 2 and 3 touch at $\vec{k} = \pm(2\pi/(3\sqrt{3}), -2\pi/3)$; further, the bottom band is dispersionless in this case.

Figures 2(a) and 2(c) show the bulk energy dispersion for $\Delta = 2$ and $D/J = 2/\sqrt{3}$ and $D = 4/\sqrt{3}$ respectively.

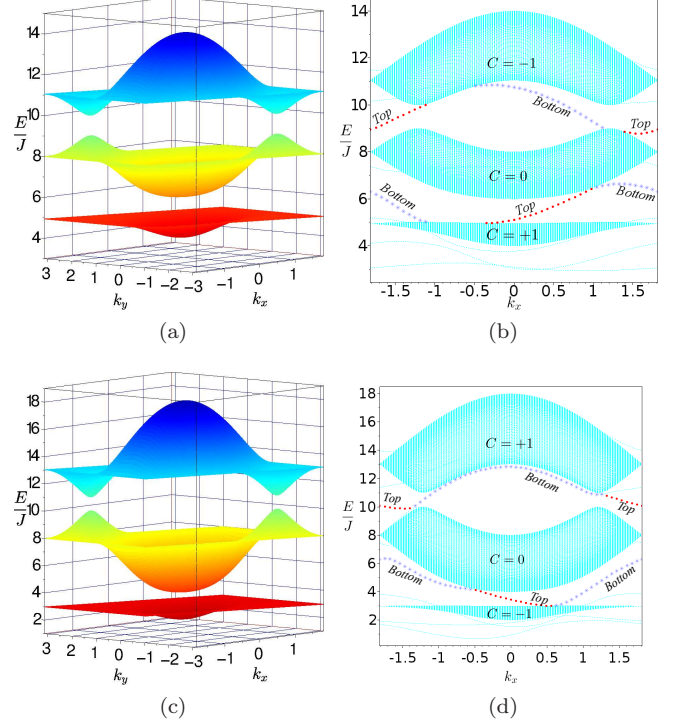


FIG. 2: Magnon energy dispersions in the bulk (a,c) and at the edges (b,d) for an infinitely long strip as shown in Fig. 1(a), in phase *I* with $\Delta = 2$. We have taken $D/J = 2/\sqrt{3}$ and $4/\sqrt{3}$ in the top and bottom rows respectively. For $D/J = 2/\sqrt{3}$ the Chern numbers for the bands with increasing energy are $(1, 0, -1)$, while for $D/J = 4/\sqrt{3}$ the Chern numbers are $(-1, 0, 1)$. A phase transition occurs at $\Delta = \sqrt{3}$ where the gaps between the bands close (Fig. 3) and the Chern number becomes ill-defined. The red (dotted) lines, marked as “Top”, show edge states localized at the top edge whereas the blue (asterisks) lines, marked as “Bottom”, show edge states at the bottom edge.

The reason for choosing these parameter values will be made clear in the following discussion about the variation of the energy gaps with the DMI strength.

We plot the DMI dependence of the energy gaps δE_{12} (between the bottom and middle bands) and δE_{23} (between the middle and top bands) for $\Delta = 2$ in Fig. 3. We find that as we increase the DMI strength D from 0 both the gaps initially increase and then decrease. At $D/J = \sqrt{3}$, the gaps close, at the same momenta as in the case of $D = 0$, before the gaps open again. For negative D , the plot is given by a mirror reflection about the line $D = 0$, i.e., the gaps depend only on the magnitude of D and not on its sign. Thus the gaps close at $D/J = -\sqrt{3}$ too. Note that the gaps are completely independent of the anisotropy ratio Δ since this appears only in the diagonal elements of $h(\vec{k})$ and therefore only

shifts all the energy levels by 4Δ .

Since there are gaps between all pairs of bands if $D/J \neq 0, \pm\sqrt{3}$, we can calculate topological invariants for the system, namely, the Chern numbers of all the bands. These Chern numbers C_i 's ($i = 1, 2, 3$ for the bottom, middle and top bands respectively) are shown in Figs. 2(b) and 2(d) for $D/J = 2/\sqrt{3}$ and $4/\sqrt{3}$. In order to calculate C_i 's, we first define the Berry curvature in band i using the normalized eigenstates $\psi_i(\vec{k})$'s and eigenvalues $E_i(\vec{k})$'s of the Hamiltonian:

$$\Omega_i(\vec{k}) = i \sum_{j \neq i} \frac{(\psi_i^\dagger(\vec{k}) \vec{\nabla}_{\vec{k}} H(\vec{k}) \psi_j(\vec{k})) \times (\psi_j^\dagger(\vec{k}) \vec{\nabla}_{\vec{k}} H(\vec{k}) \psi_i(\vec{k}))}{[E_i(\vec{k}) - E_j(\vec{k})]^2}. \quad (15)$$

The Chern number for band i can then be calculated by integrating the Berry curvature over the Brillouin zone, i.e.,

$$C_i = \frac{1}{2\pi} \int_{BZ} d^2k \Omega_i(\vec{k}). \quad (16)$$

In this work we have used the method in Ref. 22 to calculate these topological invariants.

The topological character of the bands changes whenever the band gaps close and open. For $0 < D/J < \sqrt{3}$ the bottom middle and top bands have Chern numbers equal to $(1, 0, -1)$, whereas for $D/J < \sqrt{3}$ these numbers change to $(-1, 0, 1)$ and remain so till we reach the PT line with phase II. Since the band gap closes at $D = \sqrt{3}J$ the Chern numbers are ill-defined there. A similar behavior is seen for $D < 0$. The Chern numbers are $(-1, 0, 1)$ for $-\sqrt{3} < D/J < 0$ and change to $(1, 0, -1)$ when $D/J < -\sqrt{3}$. We will now study if the Chern numbers have any implications for the edge modes of the system.

We consider a strip of the Kagome lattice which is infinitely long in the \hat{x} direction (this is the same as the \hat{n}_1 direction). This makes k_x (and hence k_1) a good quantum number. We take the width of the strip N_2 in the \hat{n}_2 direction to be about 150 unit cells; each unit cell consists of a triangle of three spins as usual; see Fig. 1(a). This reduces the lattice to a series of one-dimensional chains; each chain has N_2 unit cells (and therefore $3N_2$ sites) and is coupled to its neighboring chains. Each chain is labeled by the value of n_1 , and the magnon wave functions at all the sites of the chain carry a plane wave factor equal to $e^{ik_1 n_1}$. The wave functions on adjacent chains are therefore related to each other by plane wave factors equal to $e^{\pm ik_1}$. We can then construct a $3N_2 \times 3N_2$ Hamiltonian for each value of k_1 whose eigenvalues are the energies at that k_1 . The spectra of edge modes are shown in Figs. 2(b) and 2(d) for $\Delta = 2$ and $D/J = 2/\sqrt{3}$ and $4/\sqrt{3}$ respectively. We note that the energy spectra are quite different for modes localized near the top and

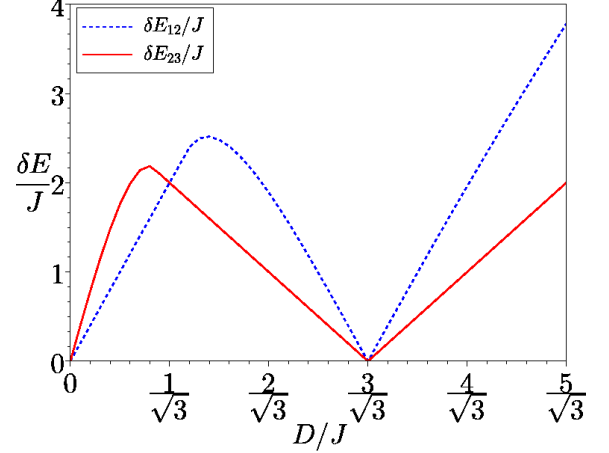


FIG. 3: Gap between bottom and middle bands, $\delta E_{12}/J$, and between middle and top bands, $\delta E_{23}/J$, as a function of D/J in the ferromagnetic phase in which all the spins point along the $+\hat{z}$ or $-\hat{z}$ direction. The gaps vanish at $D/J = 0$ and $\sqrt{3}$. We have taken $\Delta = 2$.

bottom edges; this is because the shapes of these edges are different from each other as we see in Fig. 1(a).

Since the system is topological away from the lines $D/J = 0, \pm\sqrt{3}$, the edge states are topologically protected. We find that the number of edge states ν_i at either the top edge or the bottom edge with energies in the i -th band gap is related to the Chern number up to the i -th band as^{7,23,24}

$$\nu_i = \left| \sum_{j \leq i} C_j \right|. \quad (17)$$

This is reflected in the edge state spectra in Figs. 2(b) and 2(d).

C. Thermal Hall Conductivity

The thermal Hall conductivity κ^{xy} of the system is closely related to Berry curvature $\Omega_i(\vec{k})$ of the i th band of the system as

$$\kappa^{xy} = - \frac{k_B^2 T}{4\pi^2 \hbar} \sum_i \int_{BZ} d^2k c_2(\rho_i(\vec{k})) \Omega_i(\vec{k}), \quad (18)$$

where T is the temperature, k_B is the Boltzmann constant, \hbar is Planck's constant, and i denotes the band index, i.e., $i = 1, 2$ and 3 for the bottom, middle and top bands respectively. In Eq. (18), the function c_2 is given by

$$c_2(x) = (1+x) \left(\ln \frac{1+x}{x} \right)^2 - (\ln x)^2 - 2\text{Li}_2(-x), \quad (19)$$

where Li_2 is the dilogarithm function

$$\text{Li}_2(z) = - \int_0^z du \frac{\ln(1-u)}{u}, \quad (20)$$

and the argument of c_2 is $\rho_i(\vec{k})$ which is equal to the Bose distribution function for the energy $E_i(\vec{k})$, i.e.,

$$\rho_i(\vec{k}) = \frac{1}{e^{E_i(\vec{k})/(k_B T)} - 1}. \quad (21)$$

Since the thermal Hall conductivity directly depends on the Berry curvature, we expect it to behave differently in different topological phases.

Figure 4 shows the variation of κ^{xy} with the temperature T and the DMI strength D . As shown in Fig. 4(a), whenever we cross a topological phase boundary, i.e., at $D/J = 0, \pm\sqrt{3}$, there is a discontinuity in κ^{xy} . These are exactly the points where the Chern numbers of the bands change. Since κ^{xy} flips sign at these points, the discontinuity is larger at higher temperatures.

We note that κ^{xy} is a monotonic function of T for a given value of D . For $D/J = -4/\sqrt{3}$ and $1/\sqrt{3}$, the κ^{xy} decreases and goes as $-T \log(T)$ for large T . At both these values of D/J the three energy bands have Chern numbers $(+1, 0, -1)$. Similarly, when $D/J = -1/\sqrt{3}$ or $D/J = 4/\sqrt{3}$, the bands have the opposite Chern numbers and κ^{xy} now increases as $T \log(T)$ with increasing T . This behavior is shown in Fig. 4(b). For all values of D , $\kappa^{xy} \rightarrow 0$ exponentially fast as $T \rightarrow 0$.

The surface plot Fig. 4(c) makes the connection between Chern number and Hall conductivity clearer. The regions where the Chern numbers are $(+1, 0, -1)$, i.e., for $-5/\sqrt{3} < D/J < -\sqrt{3}$ or $0 < D/J < \sqrt{3}$, κ^{xy} decreases with increasing temperature T . These are the darker (red) regions in the figure. On the other hand, when $-\sqrt{3} < D/J < 0$ or $\sqrt{3} < D/J < 5/\sqrt{3}$ and the Chern numbers are $(-1, 0, +1)$, κ^{xy} increases with T . The lighter (yellow) regions in the figure show the behavior of κ^{xy} in this regime.

D. Phase I for finite spin

An interesting fact about phase I, which is not true for phases II – V, is that all the results discussed above remain valid for *any* value of the spin S , not just large S . To see this we first note that the total spin component along the \hat{z} direction, namely,

$$S^z = \sum_{\vec{n}} (A_{\vec{n}}^z + B_{\vec{n}}^z + C_{\vec{n}}^z) \quad (22)$$

commutes with the Hamiltonian H in Eq. (1) and can therefore be used to label the eigenstates of H . Next, the

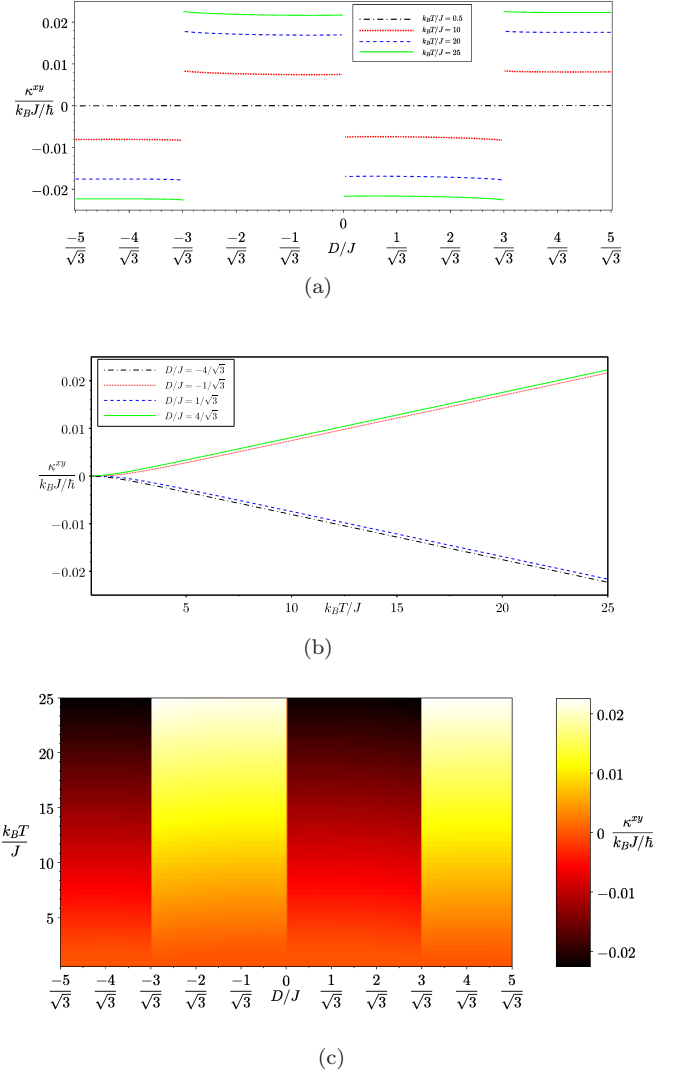


FIG. 4: Variation of κ^{xy} with temperature T and DMI strength D . (a) Varying D/J while keeping T constant, we find that at every phase transition point, i.e., at $D/J = 0, \pm\sqrt{3}$, the Hall conductivity κ^{xy} changes sign. (b) For a given value of D/J , κ^{xy} increases monotonically with temperature. We have used four different values of D/J as shown in the legend. (c) Color plot of κ^{xy} vs D/J and $k_B T/J$. The darker (red) regions where κ^{xy} becomes more and more negative with increasing temperature are where the Chern numbers are $(+1, 0, -1)$, whereas the lighter (yellow) regions where κ^{xy} increases with temperature are where the Chern numbers are $(-1, 0, +1)$.

sector with the maximum or minimum possible value of S^z , namely, the state in which all the spins have $S_i^z = S\hbar$ (or $-S\hbar$) is an exact eigenstate of H ; here i includes both the unit cell index \vec{n} and the site index A, B, C . Next, we can find the region where this state is the ground state of

H as follows. We calculate the energy of the states in the sector in which one of the spins has $S_i^z = (S-1)\hbar$ and all the other spins have $S_i^z = S\hbar$; we will call this the one-magnon sector. In this sector, the magnon annihilation and creation operators $a_{\vec{n}}$ and $a_{\vec{n}}^\dagger$ are exactly given by $A_{\vec{n}}^+ = \sqrt{2S}a_{\vec{n}}$ and $A_{\vec{n}}^- = \sqrt{2S}a_{\vec{n}}^\dagger$, and similarly, for $b_{\vec{n}}$, $c_{\vec{n}}$, etc. We then find that the Hamiltonian for a magnon is given by Eqs. (6-7) exactly, i.e., with no corrections at higher orders in a $1/S$ expansion. The form of the magnon spectrum and the locations of the boundaries of phase I are therefore identical to what we found in the large S limit. The existence of four distinct topological phases within phase I also holds for all values of S .

IV. SPIN WAVE ANALYSIS IN PHASES II AND III

In both phases II and III , all the spins lie in the same plane in the classical ground state. In phase II ($-2 \leq \Delta \leq 1$, $|D/J| \leq \sqrt{3}$), the classical ground state has all the spins pointing along the \hat{x} direction. For the spin wave analysis, we use the following Holstein-Primakoff transformation:

$$\begin{aligned} A^x &= S - a^\dagger a, & A^+ &\simeq \sqrt{2S} a, & A^- &\simeq \sqrt{2S} a^\dagger, \\ B^x &= S - b^\dagger b, & B^+ &\simeq \sqrt{2S} b, & B^- &\simeq \sqrt{2S} b^\dagger, \\ C^x &= S - c^\dagger c, & C^+ &\simeq \sqrt{2S} c, & C^- &\simeq \sqrt{2S} c^\dagger, \end{aligned} \quad (23)$$

where

$$(A, B, C)^\pm = (A, B, C)^y \pm i (A, B, C)^z \quad (24)$$

at every site labeled by $\vec{n} = (n_1, n_2)$.

On the other hand, in the ground state of phase III , the spins at sites A , B and C are rotated at an angle $2\pi/3$ with respect to one another as shown in Fig. 1. The Holstein-Primakoff transformation in this case is similar to Eqs. (23-24), except that

$$\begin{aligned} A^\pm &= A^{-\hat{n}_2} \pm i A^{-\hat{n}'_2}, \\ B^\pm &= B^{\hat{n}_3} \pm i B^{\hat{n}'_3}, \\ C^\pm &= C^x \pm i C^y, \end{aligned} \quad (25)$$

where \hat{n}_1 and \hat{n}_2 are the directions along the $A-C$ and $A-B$ bonds of each unit cell of the lattice (as shown in Fig. 1), \hat{n}_3 points along $\hat{n}_2 - \hat{n}_1$, and the unit vector \hat{n}'_i (where $i = 2, 3$) is orthogonal to \hat{n}_i such that $\hat{n}'_i \times \hat{n}_i$ point along \hat{z} . We have not transformed the spin at site C into the new basis as this spin points along the $+\hat{x}$ direction just as in phase II . The calculation is explained in more detail in Appendix A.

Using these transformations in the Hamiltonian in Eq. (1) and substituting the Fourier transforms of the bosonic operators from Eq. (5) we get the following general form of the Hamiltonian common to both phases II and III ,

$$H(\vec{k}) = \sum_{\vec{k}} \Psi^\dagger(\vec{k}) \mathcal{M}(\vec{k}) \Psi(\vec{k}), \quad (26)$$

where Ψ is a six-component column given by

$$\Psi^\dagger(\vec{k}) = \left(a_{\vec{k}}^\dagger \ b_{\vec{k}}^\dagger \ c_{\vec{k}}^\dagger \ a_{-\vec{k}} \ b_{-\vec{k}} \ c_{-\vec{k}} \right), \quad (27)$$

and $\mathcal{M}(\vec{k})$ is a 6×6 Hermitian matrix of the form

$$\mathcal{M}(\vec{k}) = \left(4\gamma \mathbb{1}_3 - \alpha F(\vec{k}) \right) \otimes \mathbb{1}_2 - \beta F(\vec{k}) \otimes \sigma_x, \quad (28)$$

where $\mathbb{1}_n$ denotes the $n \times n$ identity matrix, the Pauli matrices are

$$\sigma_x = \begin{pmatrix} 0 & 1 \\ 1 & 0 \end{pmatrix}, \quad \sigma_y = \begin{pmatrix} 0 & -i \\ i & 0 \end{pmatrix}, \quad \sigma_z = \begin{pmatrix} 1 & 0 \\ 0 & -1 \end{pmatrix}, \quad (29)$$

and

$$F(\vec{k}) = \begin{pmatrix} 0 & f(-k_1) & f(-k_2) \\ f(k_1) & 0 & f(k_1 - k_2) \\ f(k_2) & f(k_2 - k_1) & 0 \end{pmatrix}. \quad (30)$$

Here α , β and γ are always real and depend on the parameters Δ and D . The dependence on these parameters is different in the two phases. Furthermore, the matrix $F(\vec{k})$ is Hermitian, since $f(k) = 1 + e^{ik} = f^*(-k)$. Now, we see that the modes with \vec{k} and $-\vec{k}$ are coupled to each other and the Hamiltonian is not number conserving, i.e., it has terms of the form $a_{\vec{k}}^\dagger a_{-\vec{k}}$. Hence directly diagonalizing $\mathcal{M}(\vec{k})$ will not give us the required eigenvalues and eigenvectors. Therefore we use the Heisenberg equations of motion for the bosonic operators (see Appendix B for details of the calculation) to obtain the following Hamiltonian:

$$h(\vec{k}) = \left(4\gamma \mathbb{1}_3 - \alpha F(\vec{k}) \right) \otimes \sigma_z - i\beta F(\vec{k}) \otimes \sigma_y. \quad (31)$$

Since α , β and γ are different in phases II and III , we discuss the two phases separately below.

A. Phase II

The DMI term drops out of the equations in this phase and hence the matrix $\mathcal{M}_{\vec{k}}$ depends only on the anisotropy

ratio Δ . In order to obtain the magnon spectrum we use the Heisenberg equations of motion as explained in Appendix B. This method gives us the Hamiltonian of the form $h(\vec{k})$ in Eq. (31) with $\alpha = (1 + \Delta)/2$, $\beta = (1 - \Delta)/2$ and $\gamma = 1$. We thus obtain

$$h_{II}(\vec{k}) = \left(4\mathbb{1}_3 - \frac{1 + \Delta}{2}F(\vec{k})\right) \otimes \sigma_z - i\frac{1 - \Delta}{2}F(\vec{k}) \otimes \sigma_y, \quad (32)$$

where $F(\vec{k})$ is the Hermitian matrix from Eq. (30).

We find that the spectrum in this phase has no gaps between different pairs of bands irrespective of the value of Δ , as shown in the surface plot in Fig. 5(a). The top band (which is always flat) touches the middle band at momentum $\vec{k} = (0, 0)$. The middle and bottom bands touch at two points in the Brillouin zone given by $\vec{k} = \pm(2\pi/(3\sqrt{3}), -2\pi/3)$. These are the same gap closing points as in phase *I*. Finally, the bottom band always touches $E = 0$ at momentum $\vec{k} = (0, 0)$. This corresponds to a Goldstone mode in which all the spins are rotated by the same angle while keeping them in the $x - y$ plane; as mentioned before, this is a continuous symmetry of the Hamiltonian in Eq. (1). We also note that the spectrum for phase *II* matches exactly with that of phase *I* when $\Delta = 1$ and $D = 0$, i.e., for the isotropic Heisenberg Hamiltonian without any DMI.

Since pairs of bands touch each other at some values of the momentum \vec{k} , the Berry curvature $\Omega_i(\vec{k})$ is not well defined at those values of \vec{k} . Hence the Chern numbers cannot be calculated in any of the bands.

We also calculate the edge state spectrum in this phase by considering an infinite strip along \hat{x} direction with a finite width of N_2 unit cells. We solve this by effectively reducing the system to a series of one-dimensional chains of length N_2 each, with the wave function on each chain related to the those in the neighboring chains by factors of $e^{\pm ik_1}$. Using this along with the Holstein-Primakoff transformations and Heisenberg equations of motion, we obtain a $6N_2 \times 6N_2$ spin wave Hamiltonian which we diagonalize to find the spectrum E versus k_x . The details of the edge state calculation are presented in Appendix C.

The edge state spectrum in phase *II* is shown in Fig. 5(b). The continuous bands in this figure are projections of the surface plot of the bulk spectrum in Fig. 5(a) on to the $k_x - E$ plane; thus the top band in Fig. 5(a), which is completely flat, projects on to a single line at the top of Fig. 5(b). The discrete lines in Fig. 5(b) show the edge state spectra. We see that there are states which are localized along the top edge as well as states localized along the bottom edge. However, since the bulk spectrum is gapless, the edge states in this phase are not

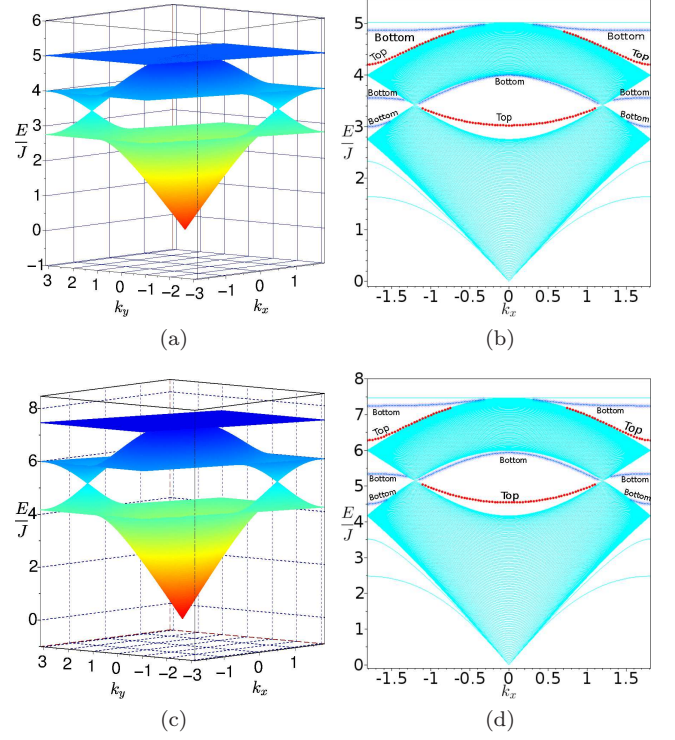


FIG. 5: Bulk and edge state spectra for phase *II* (a,b) and phase *III* (c,d). In phase *II*, the magnon spectrum is completely independent of the DMI strength; we have set $\Delta = 0.1$. In phase *III*, we set $\Delta = 0.1$ and $D/J = 4/\sqrt{3}$. The top bands in (a) and (c) are completely flat and hence appear to be a single line in the corresponding spectra shown in (b) and (d). There are no gaps between any pair of bands in either of these phases and hence the edge states are not topologically protected. The red (dotted) lines, marked as “Top”, show edge states localized at the top edge whereas the blue (asterisks) lines, marked as “Bottom”, show edge states at the bottom edge.

topologically protected in this phase.

B. Phase *III*

In this phase we again follow the same procedure with the Heisenberg equations of motion and obtain a Hamiltonian of the same form as in Eq. (31), with $\alpha = (D' + \Delta)/2$, $\beta = (D' - \Delta)/2$ and $\gamma = D'$, i.e.,

$$h_{III}(\vec{k}) = \left(4D'\mathbb{1}_3 - \frac{D' + \Delta}{2}F(\vec{k})\right) \otimes \sigma_z - i\frac{D' - \Delta}{2}F(\vec{k}) \otimes \sigma_y, \quad (33)$$

where $D' = (\sqrt{3}D/J - 1)/2$, and $F(\vec{k})$ is given in Eq. (30).

In contrast to phase *II*, the spin wave Hamiltonian here depends on both Δ and the DMI strength D . However, interestingly, the qualitative results are the same as in phase *II* as we explain below.

Diagonalizing the Hamiltonian in Eq. (33) gives the bulk spectrum shown in Fig. 5(c). In this phase too, as in phase *II*, we find a spectrum with no gaps between different pairs of bands, and a dispersionless top band. The top and middle bands touch at $\vec{k} = (0, 0)$, the middle and bottom bands touch at $\vec{k} = \pm(2\pi/(3\sqrt{3}), -2\pi/3)$, and the bottom band touches $E = 0$ at $\vec{k} = (0, 0)$ corresponding to the Goldstone mode discussed above. The gapless nature of the spectrum results in ill-defined Chern numbers; hence the edge states in this phase are not topologically protected. Figure 5(d) shows the bulk and edge state spectrum in phase *III*.

V. DISCUSSION

In this paper we have studied a spin model on the Kagome lattice with XXZ and Dzyaloshinskii-Moriya interactions between nearest-neighbor sites. In the limit of large spin S , a classical analysis shows that this system has five different phases with different ground state spin configurations. We then use the Holstein-Primakoff transformation from spins to bosons in order to go to the next order in a $1/S$ expansion; this gives the energy dispersion of the magnons in the bulk. One of the phases, called phase *I*, turns out to be rather simple; in the ground state, all the spins point in the $+\hat{z}$ or $-\hat{z}$ direction. We find that this phase consists of four distinct topological phases in which the bulk bands have different values of the Chern numbers. We have studied strips of the system which are infinitely long in one direction and have a finite width in the other direction; such a system hosts states whose wave functions are localized along one of the two edges and whose energies lie within the gaps of the bulk bands. The number of edge states is related to the Chern numbers which confirms that this phase is topological. We calculate the thermal Hall conductivity and find that this too can distinguish between the different topological phases lying within phase *I*. All these results are valid for any finite value of S , including spin-1/2. In three of the other phases (*II* – *IV*), there are no gaps between pairs of bulk bands; hence the Chern numbers of the bands cannot be calculated, and these phases are not topological. A long strip of the system again has edge states in these phases but these are not topologically protected.

It would be interesting to study the behavior of the system in more detail in phase *V*. In this phase, since the spin configuration on the three sublattices is not coplanar in the ground state, one can expect a more

complicated magnon spectrum and edge mode structure. Furthermore, even in the collinear and coplanar phases (*I* – *IV*), adding a next-nearest-neighbor interaction can significantly alter the magnon spectrum as well as the topological characters of the bands, thus affecting the behavior of the edge modes. The combined effects of anisotropy, the next-nearest-neighbor coupling and the Dzyaloshinskii-Moriya interaction may result in an even richer phase diagram. Finally, making some of the parameters of the Hamiltonian time-dependent might have interesting consequences since it is known that varying parameters in time can lead to transitions between topological and non-topological phases.

Acknowledgments

D.S. thanks Department of Science and Technology, India for Project No. SR/S2/JCB-44/2010 for financial support.

Appendix A: Holstein-Primakoff transformation in phase *III*

In this phase the ground state spins point in the directions of the vectors $-\hat{n}_2$, $\hat{n}_1 - \hat{n}_2$ and \hat{x} (as shown in Fig. 1) for sites in the *A*, *B* and *C* sublattices respectively. The directions \hat{n}_1 and \hat{n}_2 are along the *A* – *B* and *A* – *C* bonds of the unit cell. However, the Hamiltonian in Eq. (1) is written in terms of the spins in the \hat{x} and \hat{y} directions. In order to use the Holstein-Primakoff transformations in Eqs. (23) and (25), we must therefore write the Hamiltonian in terms of this new basis. If $R(\theta)$ is the rotation matrix in the $x - y$ plane, i.e.,

$$\mathcal{R}(\theta) = \begin{pmatrix} \cos \theta & -\sin \theta \\ \sin \theta & \cos \theta \end{pmatrix}, \quad (\text{A1})$$

and $\hat{n}_3 = \hat{n}_1 - \hat{n}_2$ and \hat{n}' denote the directions orthogonal to \hat{n} such that $\hat{n} \times \hat{n}'$ is along \hat{z} , then the x and y components of the spin at each site are related to the new basis as

$$\begin{pmatrix} A^x \\ A^y \end{pmatrix} = \mathcal{R}\left(\frac{2\pi}{3}\right) \begin{pmatrix} A^{-\hat{n}_2} \\ A^{-\hat{n}'_2} \end{pmatrix}, \quad (\text{A2})$$

and

$$\begin{pmatrix} B^x \\ B^y \end{pmatrix} = \mathcal{R}\left(\frac{-2\pi}{3}\right) \begin{pmatrix} B^{\hat{n}_3} \\ B^{\hat{n}'_3} \end{pmatrix}. \quad (\text{A3})$$

Since we have assumed the spins on the C sublattice to be aligned along the $+\hat{x}$ direction, we need not transform those. Therefore, the $x - y$ part of H_H in Eq. (1), i.e.,

$$H_H^{xy} = -J \sum_{\langle \vec{n}\vec{n}' \rangle} (A_{\vec{n}}^\alpha B_{\vec{n}'}^\alpha + B_{\vec{n}}^\alpha C_{\vec{n}'}^\alpha + C_{\vec{n}}^\alpha A_{\vec{n}'}^\alpha) \quad (\text{A4})$$

can be written in terms of the new basis as

$$\begin{aligned} H_H^{xy} = & -J \sum_{\langle \vec{n}\vec{n}' \rangle} \left\{ \begin{pmatrix} A_{\vec{n}}^{-\hat{n}_2} & A_{\vec{n}}^{-\hat{n}_2'} \end{pmatrix} \mathcal{R}\left(\frac{-2\pi}{3}\right) \begin{pmatrix} B_{\vec{n}'}^{\hat{n}_3} \\ B_{\vec{n}'}^{\hat{n}_3'} \end{pmatrix} \right. \\ & + \begin{pmatrix} B_{\vec{n}}^{\hat{n}_3} & B_{\vec{n}}^{\hat{n}_3'} \end{pmatrix} \mathcal{R}\left(\frac{-2\pi}{3}\right) \begin{pmatrix} C_{\vec{n}'}^x \\ C_{\vec{n}'}^y \end{pmatrix} \\ & \left. + \begin{pmatrix} C_{\vec{n}}^x & C_{\vec{n}}^y \end{pmatrix} \mathcal{R}\left(\frac{-2\pi}{3}\right) \begin{pmatrix} A_{\vec{n}'}^{-\hat{n}_2} \\ A_{\vec{n}'}^{-\hat{n}_2'} \end{pmatrix} \right\}, \quad (\text{A5}) \end{aligned}$$

where nearest neighbors are denoted by $\langle \vec{n}, \vec{n}' \rangle$. The z -part of H_H remains the same as in phase I , i.e.,

$$H_H^z = -J\Delta \sum_{\langle \vec{n}\vec{n}' \rangle} (A_{\vec{n}}^z B_{\vec{n}'}^z + B_{\vec{n}}^z C_{\vec{n}'}^z + C_{\vec{n}}^z A_{\vec{n}'}^z). \quad (\text{A6})$$

For the DMI term H_{DM} , we write terms of the type $A^x B^y - A^y B^x$ in the new basis, i.e.,

$$\begin{aligned} A^x B^y - A^y B^x &= \begin{pmatrix} A^x & A^y \end{pmatrix} \begin{pmatrix} 0 & 1 \\ -1 & 0 \end{pmatrix} \begin{pmatrix} B^x \\ B^y \end{pmatrix} \\ &= \begin{pmatrix} A^{-\hat{n}_2} & A^{-\hat{n}_2'} \end{pmatrix} \mathcal{R}\left(\frac{\pi}{6}\right) \begin{pmatrix} B^{\hat{n}_3} \\ B^{\hat{n}_3'} \end{pmatrix}. \quad (\text{A7}) \end{aligned}$$

Similarly, for the $B - C$ and $C - A$ pairs

$$B^x C^y - B^y C^x = \begin{pmatrix} B^{\hat{n}_3} & B^{\hat{n}_3'} \end{pmatrix} \mathcal{R}\left(\frac{\pi}{6}\right) \begin{pmatrix} C^x \\ C^y \end{pmatrix}, \quad (\text{A8})$$

$$C^x A^y - C^y A^x = \begin{pmatrix} C^x & C^y \end{pmatrix} \mathcal{R}\left(\frac{\pi}{6}\right) \begin{pmatrix} A^{-\hat{n}_2} \\ A^{-\hat{n}_2'} \end{pmatrix}. \quad (\text{A9})$$

This implies that

$$\begin{aligned} H_{DM} = & D \sum_{\langle \vec{n}\vec{n}' \rangle} \left\{ \begin{pmatrix} A_{\vec{n}}^{-\hat{n}_2} & A_{\vec{n}}^{-\hat{n}_2'} \end{pmatrix} \mathcal{R}\left(\frac{\pi}{6}\right) \begin{pmatrix} B_{\vec{n}'}^{\hat{n}_3} \\ B_{\vec{n}'}^{\hat{n}_3'} \end{pmatrix} \right. \\ & + \begin{pmatrix} B_{\vec{n}}^{\hat{n}_3} & B_{\vec{n}}^{\hat{n}_3'} \end{pmatrix} \mathcal{R}\left(\frac{\pi}{6}\right) \begin{pmatrix} C_{\vec{n}'}^x \\ C_{\vec{n}'}^y \end{pmatrix} \\ & \left. + \begin{pmatrix} C_{\vec{n}}^x & C_{\vec{n}}^y \end{pmatrix} \mathcal{R}\left(\frac{\pi}{6}\right) \begin{pmatrix} A_{\vec{n}'}^{-\hat{n}_2} \\ A_{\vec{n}'}^{-\hat{n}_2'} \end{pmatrix} \right\}. \quad (\text{A10}) \end{aligned}$$

Using the Holstein-Primakoff transformations in Eqs. (23) and (25) and ignoring all terms higher than second order in the bosonic creation and annihilation operators, we find that $H_{DM} \simeq -D\sqrt{3}H_H^{xy}$. Therefore, in phase III we get a very simple form of the spin wave Hamiltonian,

$$H_{III} \simeq (1 - D\sqrt{3})H_H^{xy} + H_H^z. \quad (\text{A11})$$

We then use the Fourier transform of the bosonic operators,

$$(a, b, c)_{\vec{n}} = \sum_{\vec{k}} (a, b, c)_{\vec{k}} e^{i\vec{k} \cdot \vec{n}}, \quad (\text{A12})$$

to obtain the following Hamiltonian in terms of the momentum \vec{k} ,

$$H(\vec{k}) = \sum_{\vec{k}} \Psi^\dagger(\vec{k}) \mathcal{M}(\vec{k}) \Psi(\vec{k}), \quad (\text{A13})$$

such that

$$\Psi^\dagger(\vec{k}) = \left(a_{\vec{k}}^\dagger \ b_{\vec{k}}^\dagger \ c_{\vec{k}}^\dagger \ a_{-\vec{k}} \ b_{-\vec{k}} \ c_{-\vec{k}} \right), \quad (\text{A14})$$

and $\mathcal{M}(\vec{k})$ is a 6×6 matrix

$$\begin{aligned} \mathcal{M}(\vec{k}) = & \left(4D' \mathbb{1}_3 - \frac{D' + \Delta}{2} F(\vec{k}) \right) \otimes \mathbb{1}_2 \\ & - \frac{D' - \Delta}{2} F(\vec{k}) \otimes \sigma_x, \quad (\text{A15}) \end{aligned}$$

where $D' = (\sqrt{3}D/J - 1)/2$, and $F(\vec{k})$ is given in Eq. (30). After this, we use the Heisenberg equations of motion as shown in Appendix B for further analysis.

Appendix B: Energy spectrum using Heisenberg equations of motion

Since the Hamiltonian in Eq. (A13) mixes the $+\vec{k}$ and $-\vec{k}$ modes, we use the following Heisenberg equations of

motion to calculate the magnon spectrum in phases *II* and *III*.

$$\begin{aligned} [a_{\vec{k}}^\dagger, H(\vec{k})] &= i\dot{a}_{\vec{k}}^\dagger = E a_{\vec{k}}^\dagger, \\ [b_{\vec{k}}^\dagger, H(\vec{k})] &= i\dot{b}_{\vec{k}}^\dagger = E b_{\vec{k}}^\dagger, \\ [c_{\vec{k}}^\dagger, H(\vec{k})] &= i\dot{c}_{\vec{k}}^\dagger = E c_{\vec{k}}^\dagger, \end{aligned} \quad (\text{B1})$$

where we have assumed that all the bosonic operators evolve in time as e^{-iEt} . Using $H(\vec{k})$ from Eq. (26) to calculate the commutators in Eq. (B1), we obtain the following two matrix equations,

$$\begin{pmatrix} M_{11} & M_{12} & M_{13} & M_{14} & M_{15} & M_{16} \\ M_{21} & M_{22} & M_{23} & M_{24} & M_{25} & M_{26} \\ M_{31} & M_{32} & M_{33} & M_{34} & M_{35} & M_{36} \\ -M_{41} & -M_{42} & -M_{43} & -M_{44} & -M_{45} & -M_{46} \\ -M_{51} & -M_{52} & -M_{53} & -M_{54} & -M_{55} & -M_{56} \\ -M_{61} & -M_{62} & -M_{63} & -M_{64} & -M_{65} & -M_{66} \end{pmatrix} \begin{pmatrix} a_{\vec{k}} \\ b_{\vec{k}} \\ c_{\vec{k}} \\ a_{-\vec{k}}^\dagger \\ b_{-\vec{k}}^\dagger \\ c_{-\vec{k}}^\dagger \end{pmatrix} = E \begin{pmatrix} a_{\vec{k}} \\ b_{\vec{k}} \\ c_{\vec{k}} \\ a_{-\vec{k}}^\dagger \\ b_{-\vec{k}}^\dagger \\ c_{-\vec{k}}^\dagger \end{pmatrix},$$

and

$$\begin{pmatrix} -M_{11} & -M_{21} & -M_{31} & -M_{41} & -M_{51} & -M_{61} \\ -M_{12} & -M_{22} & -M_{32} & -M_{42} & -M_{52} & -M_{62} \\ -M_{13} & -M_{23} & -M_{33} & -M_{43} & -M_{53} & -M_{63} \\ M_{14} & M_{24} & M_{34} & M_{44} & M_{54} & M_{64} \\ M_{15} & M_{25} & M_{35} & M_{45} & M_{55} & M_{65} \\ M_{16} & M_{26} & M_{36} & M_{46} & M_{56} & M_{66} \end{pmatrix} \begin{pmatrix} a_{\vec{k}}^\dagger \\ b_{\vec{k}}^\dagger \\ c_{\vec{k}}^\dagger \\ a_{-\vec{k}} \\ b_{-\vec{k}} \\ c_{-\vec{k}} \end{pmatrix} = E \begin{pmatrix} a_{\vec{k}}^\dagger \\ b_{\vec{k}}^\dagger \\ c_{\vec{k}}^\dagger \\ a_{-\vec{k}} \\ b_{-\vec{k}} \\ c_{-\vec{k}} \end{pmatrix}.$$

We can write these more compactly as

$$h\Psi(k_1) = E\Psi(k_1), \quad (\text{B2})$$

and

$$\tilde{h}\tilde{\Psi}(k_1) = \tilde{E}\tilde{\Psi}(k_1) \quad (\text{B3})$$

where $\tilde{\Psi} = (\Psi^\dagger)^T$.

Now, the matrix $\mathcal{M}(\vec{k})$ can be written as

$$\mathcal{M}(\vec{k}) = \left(4\gamma\mathbb{1}_3 - \alpha F(\vec{k}) \right) \otimes \mathbb{1}_2 - \beta F(\vec{k}) \otimes \sigma_x, \quad (\text{B4})$$

where $F(\vec{k})$ is given in Eq. (30), and α , β and γ (which are all real-valued functions of Δ and D) take different values in phases *II* and *III*. In block form, we have

$$\mathcal{M}(\vec{k}) = \begin{pmatrix} 4\gamma\mathbb{1}_3 - \alpha F(\vec{k}) & -\beta F(\vec{k}) \\ -\beta F(\vec{k}) & 4\gamma\mathbb{1}_3 - \alpha F(\vec{k}) \end{pmatrix}. \quad (\text{B5})$$

This means that the 6×6 matrix $h(\vec{k})$ in Eq. (B2) becomes

$$\begin{pmatrix} 4\gamma\mathbb{1}_3 - \alpha F(\vec{k}) & -\beta F(\vec{k}) \\ \beta F(\vec{k}) & -(4\gamma\mathbb{1}_3 - \alpha F(\vec{k})) \end{pmatrix}. \quad (\text{B6})$$

In a more compact form this is

$$h(\vec{k}) = \left(4\gamma\mathbb{1}_3 - \alpha F(\vec{k}) \right) \otimes \sigma_z - i\beta F(\vec{k}) \otimes \sigma_y, \quad (\text{B7})$$

whose eigenvalues give the magnon spectra in phases *II* and *III*.

Since $F(\vec{k}) = F^\dagger(\vec{k})$ and α and β are real, we have $h = \tilde{h}^\dagger$. Hence, diagonalizing one of these, say, $h(\vec{k})$ is sufficient to obtain the magnon spectrum.

In phase *II*, $\alpha = (1 + \Delta)/2$, $\beta = (1 - \Delta)/2$ and $\gamma = 1$ which gives us Eq. (32). The magnon spectrum in this phase is completely independent of the DMI strength D .

On the other hand, in phase *III*, $\alpha = (D' + \Delta)/2$, $\beta = (D' - \Delta)/2$ and $\gamma = D'$ where $D' = (\sqrt{3}D/J - 1)/2$ which gives us Eq. (33).

Appendix C: Calculating the edge states

We consider a strip which is N_2 unit cells wide in the \hat{n}_2 direction and is infinitely long along the \hat{x} direction (\hat{n}_1 direction). As the system is translationally invariant along \hat{n}_1 , k_1 a good quantum number; the system can be reduced to a single chain which has N_2 unit cells (i.e., $3N_2$ sites) with wave functions which are related to those of neighboring chains by factors of $e^{\pm ik_1}$. We Fourier transform the bosonic operators only in the \hat{n}_1 direction

$$(a, b, c)_{\vec{n}} = \sum_{k_1} (a, b, c)_{(k_1, n_2)} e^{ik_1 n_1}. \quad (\text{C1})$$

We then use suitable Holstein-Primakoff transformations depending upon the phase we are working in, and we retain terms only up to second order in the bosonic operators as usual.

1. Phase I

In phase *I*, the procedure described above gives us a number conserving $3N_2 \times 3N_2$ Hamiltonian which is a function of the momentum k_1 , i.e.,

$$H_I^d = \sum_{k_1} \Psi^\dagger(k_1) h(k_1) \Psi(k_1), \quad (\text{C2})$$

where

$$\Psi^\dagger_{k_1} = \left(a_{k_1,1}^\dagger \quad b_{k_1,1}^\dagger \quad c_{k_1,1}^\dagger \quad \cdots \quad a_{k_1,N_2}^\dagger \quad b_{k_1,N_2}^\dagger \quad c_{k_1,N_2}^\dagger \right). \quad (\text{C3})$$

Here the site index n_2 increases from bottom to top along the direction \hat{n}_2 , i.e., the sites on the lower edge are labeled as $n_2 = 1$ while at the top edge have $n_2 = N_2$. Diagonalizing $h(k_1)$ gives us the energy levels and wave functions of the bulk as well as edge states as functions of momentum k_1 .

2. Phases II and III

In this case we get a non-number conserving Hamiltonian which is a $6N_2 \times 6N_2$ matrix that mixes the $+k_1$ and $-k_1$ modes, i.e.,

$$H^{1d} = \sum_{k_1} \Psi^\dagger(k_1) \mathcal{M}^{1d}(k_1) \Psi(k_1), \quad (C4)$$

where the row vector $\Psi^\dagger(k_1)$ has $6N_2$ components given by

$$\begin{aligned} \Psi^\dagger(k_1) = & \left(a_{k_1,1}^\dagger \quad b_{k_1,1}^\dagger \quad c_{k_1,1}^\dagger \quad a_{-k_1,1} \quad b_{-k_1,1} \quad c_{-k_1,1} \right. \\ & \cdots \quad a_{k_1,N_2}^\dagger \quad b_{k_1,N_2}^\dagger \quad c_{k_1,N_2}^\dagger \quad a_{-k_1,N_2} \quad b_{-k_1,N_2} \quad c_{-k_1,N_2} \Big). \end{aligned} \quad (C5)$$

We again use the Heisenberg equations of motion for the bosonic operators at each site of the chain along the \hat{n}_2 direction,

$$\begin{aligned} \left[a_{\pm k_1, n_2}^\dagger, H^{1d}(k_1) \right] &= i\dot{a}_{\pm k_1, n_2}^\dagger = E a_{\pm k_1, n_2}^\dagger, \\ \left[b_{\pm k_1, n_2}^\dagger, H^{1d}(k_1) \right] &= i\dot{b}_{\pm k_1, n_2}^\dagger = E b_{\pm k_1, n_2}^\dagger, \\ \left[c_{\pm k_1, n_2}^\dagger, H^{1d}(k_1) \right] &= i\dot{c}_{\pm k_1, n_2}^\dagger = E c_{\pm k_1, n_2}^\dagger \end{aligned} \quad (C6)$$

to obtain the spectrum E versus k_x . This gives us two sets of matrix equations similar to Eqs. (B2), except that now we have $6N_2$ components instead of just six, i.e.,

$$h^{1d}(k_1) \Psi(k_1) = E \Psi(k_1), \quad (C7)$$

and

$$\tilde{h}^{1d}(k_1) \tilde{\Psi}(k_1) = \tilde{E} \tilde{\Psi}(k_1), \quad (C8)$$

where $\tilde{\Psi} = (\Psi^\dagger)^T$, and h^{1d} and \tilde{h}^{1d} are related to each other by Hermitian conjugation. Diagonalizing either one of these $6N_2 \times 6N_2$ matrices (either $h^{1d}(k_1)$ or $\tilde{h}^{1d}(k_1)$) gives us the spectrum E versus k_1 , and hence E versus k_x , since $k_x = k_1/\sqrt{3}$.

-
- ¹ X.-L. Qi and S.-C. Zhang, Rev. Mod. Phys. **83**, 1057 (2011).
² A. B. Khanikaev, S. H. Mousavi, W.-K. Tse, M. Kargarian, A. H. MacDonald, and G. Shvets, Nature Materials **12**, 233 (2013).
³ S. H. Mousavi, A. B. Khanikaev, and Z. Wang, Nature Communications **6**, 8682 (2015).
⁴ Y. Onose, T. Ideue, H. Katsura, Y. Shiomi, N. Nagaosa, and Y. Tokura, Science **329**, 297 (2010).
⁵ L. Zhang, J. Ren, J.-S. Wang, and B. Li, Phys. Rev. B **87**, 144101 (2013).
⁶ A. Mook, J. Henk, and I. Mertig, Phys. Rev. B **89**, 134409 (2014).
⁷ A. Mook, J. Henk, and I. Mertig, Phys. Rev. B **90**, 024412 (2014).
⁸ R. Chisnell, J. S. Helton, D. E. Freedman, D. K. Singh, R. I. Bewley, D. G. Nocera, and Y. S. Lee, Phys. Rev. Lett. **115**, 147201 (2015).
⁹ S. A. Owerre, Phys. Rev. B **95**, 014422 (2017).
¹⁰ S. A. Owerre, J. Phys. Commun. **1**, 021002 (2017).
¹¹ S. El-Hog, H. T. Diep, and H. Puzskarski, J. Phys. Condens. Matter **29**, 305001 (2017).
¹² N. Okuma, Phys. Rev. Lett. **119**, 107205 (2017).
¹³ S. S. Pershoguba, S. Banerjee, J.C. Lashley, J. Park, H. Agren, G. Aepli, and A. V. Balatsky, arXiv:1706.03384.
¹⁴ K. Nakata, J. Klinovaja, and D. Loss, Phys. Rev. B **95**, 125429 (2017).
¹⁵ K. Nakata, S. K. Kim, J. Klinovaja, and D. Loss, arXiv:1707.07427v2, to appear in Phys. Rev. B.
¹⁶ P. A. Pantaleón and Y. Xian, arXiv:1709.01855.
¹⁷ I. Dzyaloshinsky, J. Phys. Chem. Solids **4**, 241 (1958).
¹⁸ T. Moriya, Phys. Rev. **120**, 91 (1960).
¹⁹ R. Matsumoto and S. Murakami, Phys. Rev. Lett. **106**, 197202 (2011).
²⁰ R. Matsumoto and S. Murakami, Phys. Rev. B **84**, 184406 (2011).
²¹ P. W. Anderson, Phys. Rev. **86**, 694 (1952).
²² T. Fukui, Y. Hatsugai, and H. Suzuki, J. Phys. Soc. Jpn. **74**, 1674 (2005).
²³ Y. Hatsugai, Phys. Rev. Lett. **71**, 3697 (1993).
²⁴ Y. Hatsugai, Phys. Rev. B **48**, 11851 (1993).